RADAR POLARIMETRY

Radar polarimetry is the study of the vector nature of radar signals and how the relationships between the vector field components can be used to infer the geometry and composition of the illuminated surfaces and targets. In much the same way that a color photograph contains more information than a black-and-white image, polarimetric radar systems, those that measure the vector properties of the scattered radiation, provide much more information on the illuminated scene than do single polarization systems. The polarimetric properties of a radar target are intimately connected to the target's geometry. Spherically shaped targets, such as raindrops, respond to polarized electromagnetic radiation very differently than do the pointed corners of a building, the filamentary branches of a tree, or the waves on the ocean surface. Polarimetric radar systems quantify these differences and exploit them. For instance, polarimetry can be used to better discriminate between bursts of wind-blown rain and aircraft, between breaking water waves and submarine periscopes, and between forested and urban areas.

Polarization is a characteristic of all electromagnetic (EM) radiation. Any EM wave, regardless of which part of the spectrum it occupies, propagates through free space as a transverse wave. The electric and magnetic fields of the wave are directed perpendicular to one another and lie in a plane perpendicular to the direction of propagation. It is the direction of these fields and how they vary with time and space that define the *polarization state* of the wave. The phenomenon of polarization can be illustrated easily with polarized sunglasses. Polarized sunglasses are designed to preferentially attenuate light whose electric field is oriented horizontally, since this is the predominant polarization state of the reflected light that constitutes glare. When the glasses are oriented horizontally (as they are when they are worn), the light that passes through the lenses is essentially vertically polarized. If a second pair of glasses is placed in line with the first, little change in the transmitted light will occur until the second pair is rotated by 90°. The lenses then become cross-polarized, and the view through the cascaded lenses goes dark as the second lens blocks the polarized light passed by the first.

Most common radar systems, such as those found on ships for navigation or those used by police to monitor automobile speeds, use a single antenna and thus a single polarization. These systems transmit a pulse with a polarization state determined by the antenna design. The pulse propagates out from the antenna, reflects off the target, and then propagates back to the antenna, where it is detected by the radar receiver. Although the target echo and the transmitted pulse may have different polarization states, due to changes incurred by the target's geometry or composition, only the component of the reflected echo that matches the antenna polarization will be collected. Were the target to alter the polarization state sufficiently, such that the reflected echo was orthogonal to the transmitted pulse, no echo would be detected by the radar. As in the case of the cross-polarized sunglasses, the target would be essentially invisible to this single-polarization radar. In contrast, polarimetric radar systems use multiple antennas and switches that allow a complete characterization of the reflected echo while allowing variation in the transmitted polarization as well. In fact, a fully polarimetric system can determine the echo for *any* combination of transmit and receive polarizations using only a small number (at most four) of judiciously chosen measurements.

Radar systems require more than multiple antennas and switches to operate polarimetrically. Another important aspect of a polarimetric radar system is *coherence*. Determination of the polarization state of an EM wave requires specification of both the relative magnitudes of the EM field components as well as their relative phases. A radar is coherent if it can measure the relative phase, as well as magnitude, of received echoes, and thus polarimetric radars must be coherent. (An exception to this rule is discussed in the last section of this article.) *Relative phase* indicates the timing of one EM wave component relative to another, specifying whether the vertically polarized component reaches its peak when the horizontal is near its minimum, for instance. This timing difference contains information on the structure and composition of the target.

Relative phase is also crucial if the response of a target to an arbitrary combination of transmit and receive polarizations is to be mathematically synthesized, rather than directly measured. This process is called *polarization synthesis*. From a small set of coherent measurements utilizing orthogonal polarizations (e.g., vertical and horizontal), polarization synthesis computes the radar cross section (RCS) of a given target for *any* desired combination of transmit and receive polarizations. No additional measurements of the target are needed. The results of polarization synthesis indicate which polarization combinations enhance the visibility of the target and which combinations reduce the backscatter from other, undesired objects (often referred to as *clutter*). In addition, a plot of the RCS as a function of the receive and transmit polarizations forms a *polarization signature*, which may indicate the basic geometry of the target.

Just how much can be learned about an object or a surface from its polarimetric properties is still an area of active research, particularly in the remote sensing community. Airborne polarimetric radars are being investigated as tools for monitoring land use, classifying terrain, topographic mapping, and imaging of the ocean surface. The mathematical tools that aid in the analysis and interpretation of polarimetric data are under development as well. These tools allow decomposition of a complicated scene into simpler, canonical structures that indicate the nature of the predominant scattering centers.

The following sections describe radar polarimetry in more detail. In the next section, the basic mathematical framework of polarimetry is presented, including the representation of polarized EM fields and of the polarimetric response. Important aspects of polarimetric system design are then discussed, and the article concludes with a summary of current research topics.

J. Webster (ed.), *Wiley Encyclopedia of Electrical and Electronics Engineering*.

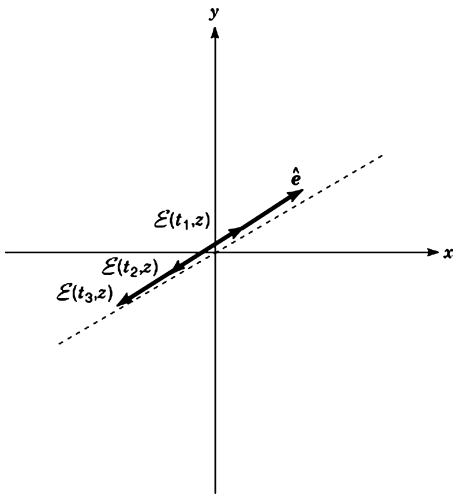

Figure 1. Electric field at three instants in time for a linearly polarized EM wave. The electric field vector is always parallel to a line defined by the vector ê. The direction of ê depends on the relative magnitudes of the x and y components of the field.

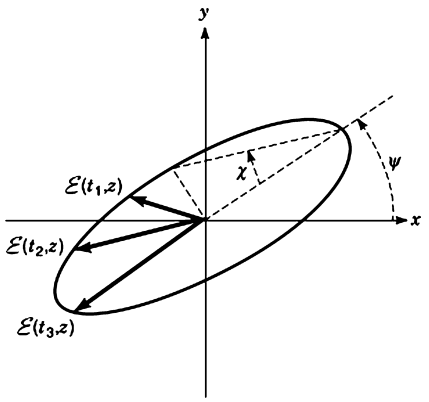

Figure 2. Electric field at three instants in time for an elliptically polarized EM wave. The tip of the electric field vector traces out an ellipse as time progresses. The ellipse is characterized by its orientation angle ψ and its ellipticity angle χ.

MATHEMATICAL FOUNDATION

Representation of Polarized Electromagnetic Waves

Completely Polarized Waves. The polarization state of an EM wave is determined by the relative magnitudes and phases of its electric field components. Assume a plane EM wave is propagating along the z-axis of a right-handed coordinate system. The electric field lies in the x–y plane and can be expressed as

$$\mathcal{E} = E_x^o \cos(\omega t - kz + \alpha_x)\hat{x} + E_y^o \cos(\omega t - kz + \alpha_y)\hat{y} \qquad (1)$$

where $\omega = 2\pi f$ is the radian frequency, $k = 2\pi/\lambda$ is the wavenumber, λ is the wavelength, t is time, and $\hat{x}$ and $\hat{y}$ are unit vectors in the x and y directions, respectively. α_x and α_y are the phases of the x and y components, and the corresponding magnitudes are $E^o{}_x$ and $E^o{}_y$.

The wave is said to be *linearly polarized* if $\alpha_x = \alpha_y = \alpha$. In this case, the two components are in phase with one another and Eq. (1) can be simplified to

$$\begin{aligned}\mathcal{E} &= \cos(\omega t - kz + \alpha) \cdot (E_x^o \hat{x} + E_y^o \hat{y}) \\ &= E^o \cos(\omega t - kz + \alpha) \cdot \hat{e}\end{aligned} \qquad (2)$$

where

$$E^o = \sqrt{(E_x^o)^2 + (E_y^o)^2} \qquad (3)$$

$$\hat{e} = (E_x^o \hat{x} + E_y^o \hat{y})/E^o \qquad (4)$$

In this case, the field is always parallel to the unit vector $\hat{e}$, as illustrated in Fig. 1. As the magnitude and sign of the field vary with time and/or position, the tip of the field vector traces out a straight line parallel to $\hat{e}$.

Elliptical polarization results when $\alpha_x \neq \alpha_y$. In this more general case, the two components are no longer in phase and the direction of the electric field is no longer constant. The tip of the electric field vector at any point in space (value of z) traces out an ellipse as time progresses. This can be illustrated by evaluating Eq. (1) at a particular value of z, for example, $z = 0$:

$$\mathcal{E}(z=0) = E_x^o \cos(\omega t + \alpha_x)\hat{x} + E_y^o \cos(\omega t + \alpha_y)\hat{y} \qquad (5)$$

This ellipse is illustrated in Fig. 2. The ellipse is characterized by its *orientation angle* ψ and *ellipticity angle* χ. In terms of the original x and y amplitudes and phases, ψ and χ are given by

$$\begin{aligned}\tan(2\psi) &= \tan(2\xi) \cdot \cos(\delta) \\ \sin(2\chi) &= \sin(2\xi) \cdot \sin(\delta)\end{aligned} \qquad (6)$$

where

$$\tan(\xi) = E_y^o / E_x^o \qquad (7)$$

and

$$\delta = \alpha_y - \alpha_x \qquad (8)$$

Note that ψ is defined as the smallest angle between the x axis and the major axis of the ellipse. The ellipticity angle can be related to the major and minor axes of the ellipse, $2E^o{}_{x'}$ and $2E^o{}_{y'}$, respectively, through the expression

$$\tan(\chi) = \mp E_{y'}^o / E_{x'}^o \qquad (9)$$

With these definitions, the limits of χ are $-45^\circ \leq \chi \leq 45^\circ$ while ψ spans the range $-90^\circ \leq \psi \leq 90^\circ$. The direction of rotation of the electric field vector about the ellipse is specified by the sign of χ. By IEEE convention, left-hand elliptical polarization is specified by $\chi > 0$, while right-hand rotation is denoted by $\chi < 0$. Note that if $|\chi| = 45^\circ$, the ellipse degenerates to a circle. This special case is referred to as *circular polarization*.

Vector notation is a convenient way to denote polarized fields. In vector exponential form, Eq. (1) can be written as

$$\mathcal{E} = \mathrm{Re}\left\{ e^{-j(\omega t - kz + \alpha_y)} \begin{bmatrix} E_x^o e^{j\delta} \\ E_y^o \end{bmatrix} \right\} = \mathrm{Re}\{e^{-j(\omega t - kz + \alpha_y)} \boldsymbol{E}\} \qquad (10)$$

where

$$\boldsymbol{E} = \begin{bmatrix} E_x^o e^{j\delta} \\ E_y^o \end{bmatrix} \equiv \begin{bmatrix} E_x \\ E_y \end{bmatrix} \qquad (11)$$

completely defines the polarization state of the wave. When a polarized electromagnetic wave is expressed in the vector form of Eq. (11), the time harmonic factor $e^{-j(\omega t - kz)}$ is assumed. The phase factor $e^{-j\alpha_y}$ in Eq. (10) can be dropped, since the value of α_y depends on the arbitrary choice of a phase reference. The polarization state can be defined even more compactly by the complex polarization ratio, $P = E_y/E_x$. All aspects of a polarized wave (except for field strength) can be expressed in terms of this single, complex number 1.

The *Stokes vector* is an alternative representation of polarized fields, defined in the following manner:

$$\boldsymbol{F} = \begin{bmatrix} |E_x|^2 + |E_y|^2 \\ |E_x|^2 - |E_y|^2 \\ 2\mathrm{Re}(E_x E_y^*) \\ 2\mathrm{Im}(E_x E_y^*) \end{bmatrix} = \begin{bmatrix} I_o \\ Q \\ U \\ V \end{bmatrix} \tag{12}$$

[The Stokes vector is sometimes defined with the element V in the second position within the vector:

$$\boldsymbol{F} = \begin{bmatrix} |E_x|^2 + |E_y|^2 \\ 2\mathrm{Im}(E_x E_y^*) \\ |E_x|^2 - |E_y|^2 \\ 2\mathrm{Re}(E_x E_y^*) \end{bmatrix}$$

In addition, some authors define $V = 2\mathrm{Im}(E^*{}_x E_y) = (-1)\cdot 2\mathrm{Im}(E_x E^*{}_y)$.] While the representations in Eqs. (11) and (12) contain the same information about wave polarization in the case of a completely polarized wave, the Stokes vector has the advantage that all the vector elements are real-valued, and, as discussed in the following section, it can accommodate fields that are not completely polarized.

For completely polarized waves, it can be shown that $I^2{}_0 = Q^2 + U^2 + V^2$. This is the equation of a sphere of radius I_0. Each polarization state can thus be mapped uniquely onto a point of a sphere, using the parameters Q,U,V as Cartesian coordinates. This graphical representation of wave polarization is referred to as the *Poincaré sphere* (1).

Partial Polarization. Not all polarized EM waves can be adequately described using the representation of Eq. (11). The polarization state of natural EM waves, such as sunlight, is unpolarized, meaning that the polarization state varies randomly from one time instant to the next. Similarly, the polarization state of the radar backscatter from some surfaces, such as the sea surface or a wind-blown canopy of trees, may vary rapidly with time. The total radar backscatter in these cases is the vector sum of many individual echoes produced by many discrete scattering centers located within the radar footprint, each of which is moving and evolving. The net polarization state may be nearly linear at one instant, but elliptical only a few milliseconds later. Even if these surfaces could be frozen in time, the polarization state would still vary appreciably as the radar beam was moved about in space, since new scattering centers would enter the spot illuminated by the beam as others would exit. What is needed in these situations is a *statistical* measure of the polarization state of the wave. The Stokes vector can be adapted to these situations, in which the time and/or spatially varying fields are termed *partially polarized*.

For partially polarized waves, the ensemble averages of the Stokes vector elements, indicated by angular brackets $\langle\rangle$, are used. The Stokes vector becomes

$$\boldsymbol{F} = \begin{bmatrix} \langle |E_x|^2 + |E_y|^2 \rangle \\ \langle |E_x|^2 - |E_y|^2 \rangle \\ \langle 2\mathrm{Re}(E_x E_y^*) \rangle \\ \langle 2\mathrm{Im}(E_x E_y^*) \rangle \end{bmatrix} \tag{13}$$

The average may be over time with the radar directed at a single spot, over space if the surface is stationary, or over a mixture of time and space. The last two elements, U and V, indicate the degree of correlation between the x and y components. For a completely unpolarized wave, E_x and E_y are uncorrelated and thus $U = V = 0$.

Vertical and Horizontal Polarization. In most radar applications, it is more convenient to represent polarized waves in a spherical, rather than rectangular, coordinate system. Since the electric and magnetic fields that propagate in free space are transverse to the direction of propagation, and thus do not always lie in a convenient, fixed plane (such as the x–y plane assumed thus far), a spherical coordinate system is a more natural choice. This is illustrated in Fig. 3. The direction of propagation of the wave (formerly the $\hat{z}$ direction) is denoted by the unit vector $\hat{\boldsymbol{k}}$, while the transverse coordinate unit vectors (formerly $\hat{\boldsymbol{x}}$ and $\hat{\boldsymbol{y}}$) are $\hat{\boldsymbol{v}}$ and $\hat{\boldsymbol{h}}$. The coordinate system $(\hat{\boldsymbol{k}},\hat{\boldsymbol{v}},\hat{\mathbf{h}})$ is defined such that it coincides with the standard spherical system $(\hat{r},\hat{\theta},\hat{\phi})$. The letters **v** and **h** refer to *vertical* and *horizontal* polarization, respectively, a reference to the fact that if the θ=90° plane is assumed to be Earth's surface (as it usually is), $\hat{\boldsymbol{v}}$ contains a vertically oriented component while $\hat{\boldsymbol{h}}$ lies in a horizontal plane. In this coordinate system, a spherical wave can be expressed as

$$\boldsymbol{E} = (E_v\hat{\boldsymbol{v}} + E_h\hat{\boldsymbol{h}})\frac{e^{jk\hat{\boldsymbol{k}}\cdot\boldsymbol{r}}}{r} \tag{14}$$

where $r = r\hat{\boldsymbol{r}}$ and r is the distance from the coordinate system origin. Sufficiently far from the origin and over a small enough range of angles about the direction $\hat{\boldsymbol{k}}$, this spherical wave can be considered to be a plane wave. All the expressions derived above for a plane wave propagating in the z direction are then still valid with the x and y subscripts interchanged with "v" and "h", respectively. Note that with this transformation, the orientation angle, ψ, is defined relative to the vertical axis. Other authors use alternative conventions, however, that define ψ relative to the horizontal.

Representation of the Polarimetric Response

The previous section describes how the polarization state of an EM wave can be described mathematically. In this section, two formalisms are presented that describe how the polarization state of a wave is *altered* when it reflects off a target. The first, which applies to completely polarized waves, utilizes the *scattering matrix* to describe the target's polarimetric properties. The second, which can be

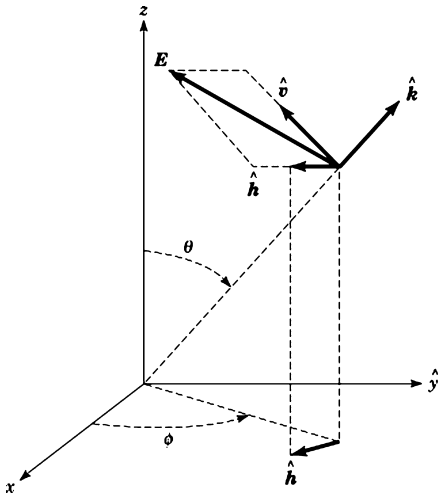

Figure 3. Diagram indicating the decomposition of the electric field $\mathcal{E}(t,z)$ into vertically and horizontally polarized components. The direction of propagation, denoted by the unit vector $\hat{k}$, and the vertically and horizontally polarized unit vectors, $\hat{v}$ and $\hat{h}$, respectively, form a right-handed coordinate system coincident with the standard spherical coordinate system $(\hat{r},\hat{\theta},\hat{\phi})$. The terms "vertical" and "horizontal" arise from the fact that $\hat{h}$ is always parallel to the horizontal ($\hat{\theta} = 90^\circ$) plane while $\hat{v}$ has a component in the vertical ($\hat{z}$) direction.

applied to completely or partially polarized targets, uses the *Mueller matrix* to describe the target. Both matrices describe the target's polarimetric properties by quantifying how the polarization of the reflected wave is related to the polarization of the incident wave, and both are *complete* descriptions of the scattering properties of the illuminated scene or target. As shown in what follows, the response of the scene to any combination of transmit and receive polarizations can be computed from these matrices, without the need for additional measurements.

When using any representation of the polarimetric response, care must be taken that consistent source, target, and receiver coordinate systems are used. This article assumes the backscatter alignment (BSA) convention in which the incident and scattered wave unit vectors are identical. For a description of other conventions, see Refs. 1 and 2. The notation used in this section closely matches that of Ref. 2.

Polarization Scattering Matrix. The scattering matrix is a 2×2 matrix relating the transmitted wave incident on a target E^t to the reflected wave at the receiver E^r:

$$\boldsymbol{E}^r = \frac{e^{jkr}}{r}\bar{\boldsymbol{S}}\boldsymbol{E}^t \tag{15}$$

where

$$\boldsymbol{E}^r = \begin{bmatrix} E_v^r \\ E_h^r \end{bmatrix} \qquad \boldsymbol{E}^t = \begin{bmatrix} E_v^t \\ E_h^t \end{bmatrix} \tag{16}$$

and

$$\bar{\boldsymbol{S}} = \begin{bmatrix} \bar{S}_{vv} & \bar{S}_{vh} \\ \bar{S}_{hv} & \bar{S}_{hh} \end{bmatrix} \tag{17}$$

is the scattering matrix. The elements of $\bar{S}$ are complex, containing both magnitude and phase information, but in most cases the four magnitudes and phases are not independent. In the case of a monostatic radar in the absence of any nonreciprocal materials (e.g., ferromagnetics or plasmas in a magnetic field), the reciprocity theorem forces $\bar{S}_{vh} = \bar{S}_{hv}$, and thus there are three independent magnitudes and two independent (relative) phases. Although not explicitly shown in Eq. (17), the elements of $\bar{S}$ are in general functions of the radar frequency as well as the orientation of the target relative to the radar system.

The variation of the scattering matrix elements with target orientation is undesirable in terms of target recognition. The task of identifying an unknown target at an unknown aspect would be much simpler if the form of its scattering matrix were essentially independent of orientation. An eigenvalue analysis of the scattering matrix can partially achieve this goal while also providing physical insight into the scattering process. Through an eigenvalue analysis (e.g., see Ref. 1), it can be shown that the scattering matrix can be diagonalized and represented by the following five independent parameters; m^2, the maximum RCS of the target; ψ_t the orientation angle; τ, the symmetry angle; ν, the bounce angle; and γ, the polarizability angle. With the exception of ψ_t, which is a direct measure of the target's rotation angle, these parameters are independent of target rotations about the radar line of sight and are thus relatively invariant indicators of a target's identity. (The parameter values will change, however, if the radar views the target from a different line of sight.) τ is a measure of the symmetry of the target, having a value of 0° for targets with a plane of symmetry and a value of $\pm 45^\circ$ for nonsymmetric objects, and is also the ellipticity angle of the eigenvectors. The bounce angle ν indicates the number of bounces involved in the target scattering, with a value of 0° corresponding to an odd number of bounces and a value of $\pm 90^\circ$ indicating an even number. Examples of odd bounce targets are spheres (one bounce) and trihedral corner reflectors (three bounces; see Example 1 below here), while the dihedral corner reflector is an even bounce scatterer (two bounces; see Example 2 here). The polarizability γ indicates the ability of the target to polarize incident radiation that is unpolarized, with 0° and 45° corresponding to complete and no polarizability, respectively. An example of a target with a high degree of polarizability is a long, thin wire, which tends to reflect only radiation polarized parallel to its axis. In contrast, a sphere exhibits $\gamma = 45^\circ$, since it has no preferred axis of symmetry. These five parameters are sometimes referred to as the Huynen parameters, in reference to their introduction by J. R. Huynen (3). These parameters also describe the *null* and *maximum polarizations* for the target, those polarization states for which the RCS is zero and m^2, respectively. When plotted on the Poincaré sphere, these polarization states define a characteristic structure called the *polarization fork* (see, e.g., Refs. 2 and 4).

In practice, the elements of the scattering matrix are generally obtained by recording the radar echoes from two pulses. First, the radar system transmits a pure vertically

polarized wave

$$\boldsymbol{E}^t = E_v^t \begin{bmatrix} 1 \\ 0 \end{bmatrix}$$

and the receiver detects and records both the vertically and horizontally polarized echoes, E_{vv} and E_{hv}. From Eqs. 15,16,17, $\bar{S}_{vv}$ and $\bar{S}_{hv}$ can then be calculated from

$$\bar{S}_{vv} = \frac{r}{e^{jkr}} \cdot \frac{E_{vv}}{E_v^t} \qquad \bar{S}_{hv} = \frac{r}{e^{jkr}} \cdot \frac{E_{hv}}{E_v^t} \tag{18}$$

Similarly, $\bar{S}_{hh}$ and $\bar{S}_{vh}$ are determined by transmitting a pure horizontally polarized pulse,

$$\boldsymbol{E}^t = E_h^t \begin{bmatrix} 0 \\ 1 \end{bmatrix}$$

and recording the vertically and horizontally polarized echoes E_{hh} and E_{vh} from which the remaining scattering matrix elements

$$\bar{S}_{hh} = \frac{r}{e^{jkr}} \cdot \frac{E_{hh}}{E_h^t} \qquad \bar{S}_{vh} = \frac{r}{e^{jkr}} \cdot \frac{E_{vh}}{E_h^t} \tag{19}$$

are obtained. Of course, two pulses of any two linearly independent polarization states could be used to determine the scattering matrix elements, since Eq. (15) defines four equations in four unknowns. But in general practice, pure vertically and horizontally polarized pulses are used.

Example 1. (Sphere) The simplest scattering matrix is that of sphere, given by

$$\bar{S}_{\text{sphere}} = A \begin{bmatrix} 1 & 0 \\ 0 & 1 \end{bmatrix} \tag{20}$$

where the constant A depends on the sphere's size. This target does not alter the polarization state of the incident radiation, since $\bar{S}_{hv} = \bar{S}_{vh} = 0$, and responds identically to horizontally and vertically polarized radiation. Other objects with scattering matrices of the same form are large, flat surfaces at normal incidence and trihedral corner reflectors. The latter is a type of radar calibration target resembling the inside corner of a box. For these targets, the Huynen parameters τ, ν, and γ are equal to 0°, 0°, and 45°, respectively, while the orientation angle ψ_t is arbitrary.

Example 2. (Rotated Dihedral Corner Reflector) A dihedral corner reflector is a radar calibration target formed from two intersecting, perpendicular plates. The scattering matrix of this target with the seam rotated at an angle θ relative to the horizontal plane is

$$\bar{S}_{\text{dihedral}} = A \begin{bmatrix} \cos(2\theta) & \sin(2\theta) \\ \sin(2\theta) & -\cos(2\theta) \end{bmatrix} \tag{21}$$

where A depends on the size of the plates. The tendency of this target to depolarize (change the polarization state of) the incident radiation is strongly dependent on its orientation. At $\theta = 22.5°$, vertically or horizontally polarized incident radiation will be rotated 45° after reflection, whereas at $\theta = 45°$, the rotation is 90°. The Huynen parameters for the dihedral are $\psi_t = \theta$, $\tau = 0°$, $\nu = 45°$, and $\gamma = 45°$.

Example 3. (Helix) The scattering matrix for a simple helix is

$$\bar{S}_{\text{helix}} = \frac{1}{2} \begin{bmatrix} -1 & \pm j \\ \pm j & 1 \end{bmatrix} \tag{22}$$

where the + and − signs refer to left- and right-handed helices, respectively. The factor $j = \sqrt{-} = e^{j\pi/2}$ arises from the natural mode of oscillation for the helix, circular polarization, in which the relative phase between the vertical and horizontal components is $\pi/2$ radians (90°). The Huynen parameters τ and γ are ±45° and 0°, respectively, while ψ_t and ν are arbitrary.

Mueller Matrix. In the same way that the scattering matrix relates the EM fields incident on and reflected from a target, the Mueller matrix relates the incident and scattered Stokes vectors

$$\boldsymbol{F}^r = \frac{1}{r^2} \bar{L} \boldsymbol{F}^t \tag{23}$$

where

$$\boldsymbol{F}^r = \begin{bmatrix} I_o^r \\ Q^r \\ U^r \\ V^r \end{bmatrix} \qquad \boldsymbol{F}^t = \begin{bmatrix} I_o^t \\ Q^t \\ U^t \\ V^t \end{bmatrix} \tag{24}$$

and $\bar{L}$ is the 4×4 Mueller matrix. Unlike in the case of the scattering matrix, the Mueller matrix elements are real. (Note that a factor of $1/r^2$ is required, rather than $1/r$ as for the scattering matrix expression, since the Stokes vector elements are proportional to products of the field components.) As shown in Ref. 2, the Mueller matrix elements can be expressed in terms of the scattering matrix elements through

$$\bar{L} = R \overline{W} R^{-1} \tag{25}$$

where

$$R = \begin{bmatrix} 1 & 1 & 0 & 0 \\ 1 & -1 & 0 & 0 \\ 0 & 0 & 1 & 1 \\ 0 & 0 & -i & i \end{bmatrix} \tag{26}$$

and

$$\overline{W} = \begin{bmatrix} \bar{S}_{vv}^* \bar{S}_{vv} & \bar{S}_{vh}^* \bar{S}_{vh} & \bar{S}_{vh}^* \bar{S}_{vv} & \bar{S}_{vv}^* \bar{S}_{vh} \\ \bar{S}_{hv}^* \bar{S}_{hv} & \bar{S}_{hh}^* \bar{S}_{hh} & \bar{S}_{hh}^* \bar{S}_{hv} & \bar{S}_{hv}^* \bar{S}_{hh} \\ \bar{S}_{hv}^* \bar{S}_{vv} & \bar{S}_{hh}^* \bar{S}_{vh} & \bar{S}_{hh}^* \bar{S}_{vv} & \bar{S}_{hv}^* \bar{S}_{vh} \\ \bar{S}_{vv}^* \bar{S}_{hv} & \bar{S}_{vh}^* \bar{S}_{hh} & \bar{S}_{vh}^* \bar{S}_{hv} & \bar{S}_{vv}^* \bar{S}_{hh} \end{bmatrix} \tag{27}$$

This relationship between $\bar{L}$ and $\bar{S}$ is strictly valid only for completely polarized targets, since $\bar{S}$ does not exist otherwise. Complex radar targets, such as wind-blown trees, exhibit time-varying polarization matrix elements, and no single scattering matrix can describe their polarization transformation properties. The elements of $\bar{S}$ tend to be zero-mean quantities, and so averaging these terms is not an effective way to describe the average polarization scattering behavior of a target. This average behavior can be described by computing a time-averaged Mueller matrix, however. In practice, the average Mueller matrix is sometimes calculated by first computing the scattering matrix

elements from each pair of a large number of alternating vertically and horizontally polarized transmit pulses, using Eqs. (18) and (19). Equations (26) and (27) are then used to compute individual Mueller matrices for each measurement. The final, averaged Mueller matrix is then calculated by averaging the individual matrix elements. This procedure is valid if the target or scene of interest can be considered to be stationary, and thus completely polarized, over the time period required to transmit a single pair of vertically and horizontally polarized pulses. As this interval can be as short as a fraction of a millisecond, this is a very reasonable assumption in many cases. A direct technique for computing the time-averaged Mueller matrix, without calculating a sequence of polarization scattering matrices, is described in Ref. 5.

Some authors use different names for the matrix $\bar{L}$ defined using the BSA convention and that defined using the forwardscatter alignment (FSA) convention, referring to the former as the *Kennaugh matrix* and the latter as the *Mueller matrix* (1). While making this distinction avoids potential confusion, both are commonly referred to as the Mueller matrix.

Other Representations of the Polarimetric Response. In addition to the scattering and Mueller matrix formalisms, the polarimetric scattering properties of the target can also be expressed by the covariance matrix **C** and the coherency (or density) matrix ρ. In terms of the scattering matrix elements, these matrices are given by

$$C = \begin{bmatrix} \bar{S}_{vv}\bar{S}_{vv}^* & \sqrt{2}\bar{S}_{vv}\bar{S}_{vh}^* & \bar{S}_{vv}\bar{S}_{hh}^* \\ \sqrt{2}\bar{S}_{vh}\bar{S}_{vv}^* & 2\bar{S}_{vh}\bar{S}_{vh}^* & \sqrt{2}\bar{S}_{vh}\bar{S}_{hh}^* \\ \bar{S}_{hh}\bar{S}_{vv}^* & \sqrt{2}\bar{S}_{hh}\bar{S}_{vh}^* & \bar{S}_{hh}\bar{S}_{hh}^* \end{bmatrix} \tag{28}$$

$$\rho = \begin{bmatrix} aa^* & ab^* & ac^* \\ ba^* & bb^* & bc^* \\ ca^* & cb^* & cc^* \end{bmatrix} \tag{29}$$

where

$$a = \frac{\bar{S}_{vv} + \bar{S}_{hh}}{2} \qquad b = \frac{\bar{S}_{vv} - \bar{S}_{hh}}{2} \qquad c = \bar{S}_{vh} = \bar{S}_{hv} \tag{30}$$

(These expressions apply to the backscattering, reciprocal case. In the general bistatic case, both **C** and ρ are 4×4 matrices.) As in the case of the Mueller matrix, these matrices can be applied to the partially polarized case through averaging of the elements, and they contain the same information as do the scattering or Mueller matrices. Different aspects of polarimetry are expressed more compactly with one representation or the other, however. (See, e.g., Refs. 2 and 4.)

Polarization Synthesis. The scattering and Mueller matrices are complete representations of the polarimetric scattering properties of a target or surface in that the target response to any combination of transmit and receive polarizations can be computed from them. *Polarization synthesis* refers to the process of determining a target's response to an arbitrary combination of transmit and receive polarizations by way of the target's scattering or Mueller matrix, without actually transmitting and receiving these polarization states.

The equation describing polarization synthesis can be derived by starting with the definition of the (monostatic) RCS of a target

$$\sigma = 4\pi \lim_{r\to\infty} r^2 \left(\frac{\boldsymbol{E}^s \cdot \boldsymbol{E}^{s*}}{\boldsymbol{E}^t \cdot \boldsymbol{E}^{t*}} \right) = 4\pi \lim_{r\to\infty} r^2 \left(\frac{|\boldsymbol{E}^s|^2}{|\boldsymbol{E}^t|^2} \right) \tag{31}$$

where $|E^s|^2$ is the electric field intensity scattered by the target, measured at the receiver, and $|E^t|^2$ is the incident electric field intensity, measured at the target, and r is the distance between the radar antenna and the target. This expression states that the RCS is given by the power per unit solid angle incident on the antenna divided by the power per unit area incident on the target.

As it stands, this expression does not account for the polarization of the receive antenna. A system will measure this value of the RCS only if the receive antenna is designed to receive the polarization state of E^s. Otherwise, only a fraction of the power incident on the antenna will be actually absorbed, and the measured RCS will be lower than that given by Eq. (31). This effect can be accounted for in the following way. The polarization of an antenna is defined by the unit vector **p**, the polarization vector, given by

$$\boldsymbol{p} = \frac{\boldsymbol{E}}{|\boldsymbol{E}|} \tag{32}$$

where, by IEEE convention, E is the far field radiated by the antenna when it is used to transmit. If a field E^s impinges on a receive antenna having polarization p^r, the effective field incident on the antenna is the projection of E^s on p^r, $p^r \cdot E^s$ and the effective field intensity is then $|p^r \cdot E^s|^2$. The expression for the cross section in this case is

$$\sigma_{rt} = 4\pi \lim_{r\to\infty} r^2 \left(\frac{|\boldsymbol{p}^r \cdot \boldsymbol{E}^s|^2}{|\boldsymbol{E}^t|^2} \right) \tag{33}$$

Noting that

$$\boldsymbol{E}^s = \frac{e^{jkr}}{r} \bar{S} \boldsymbol{E}^t$$

and making the substitution $p^t = (E^t/|E^t|)$ produces the polarization synthesis equation:

$$\sigma_{rt} = |\boldsymbol{p}^r \cdot \bar{S} \boldsymbol{p}^t|^2 \tag{34}$$

Once $\bar{S}$ has been determined, the target RCS for *any* combination of transmit and receive polarizations can be computed from this expression. The unit vectors p^r and p^t corresponding to the desired transmit and receive polarizations are simply inserted. A similar expression using the Stokes vector and Mueller matrix representation can also be derived (2).

Polarization Response. The RCS values computed by Eq. (34) can be represented graphically by a surface termed the *polarization signature* or *polarization response* (6). The term *signature* refers to the fact that these surfaces are

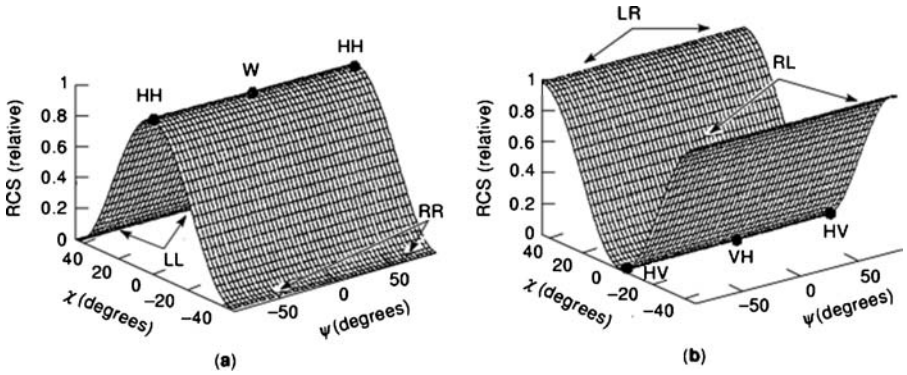

Figure 4. (a) Copolarized signature for a sphere. The surface is a plot of the normalized RCS of the sphere versus the orientation and ellipticity angles of the transmit and receive polarizations. The cross section is maximum for linearly polarized radiation, as indicated by the ridge in the surface for $\chi = 0$, and vanishes for left- and right-handed circular polarization ($\chi = \pm 45^\circ$). (b) Cross-polarized signature for the sphere. The cross-polarized signature is a plot of the normalized RCS of the sphere versus the orientation and ellipticity angles of the transmit polarization, assuming that the transmit and receive antennas are orthogonally polarized. The cross-polarized RCS vanishes for linear polarization and is maximized for left- and right-handed circular polarization.

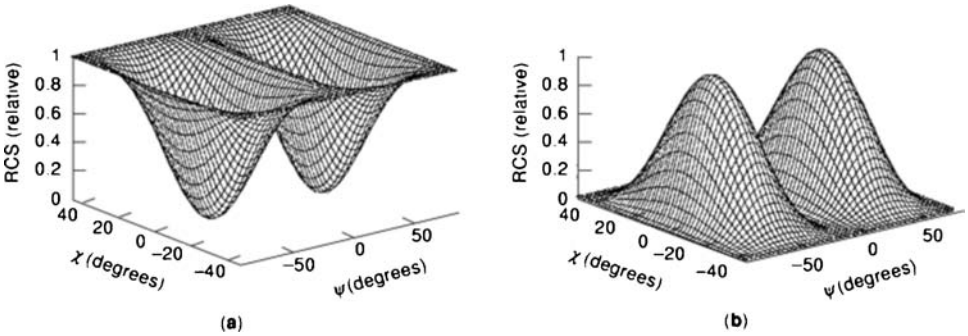

Figure 5. (a) Copolarized signature for a dihedral corner reflector with its seam oriented horizontally. The RCS is maximum for vertical, horizontal, and circular polarizations and vanishes for linear polarizations with $\psi = \pm 45^\circ$. (b) Cross-polarized signature for the dihedral corner reflector. The cross-polarized RCS is maximum for linear polarizations with $\psi = \pm 45^\circ$ and vanishes for vertical, horizontal, and circular polarizations.

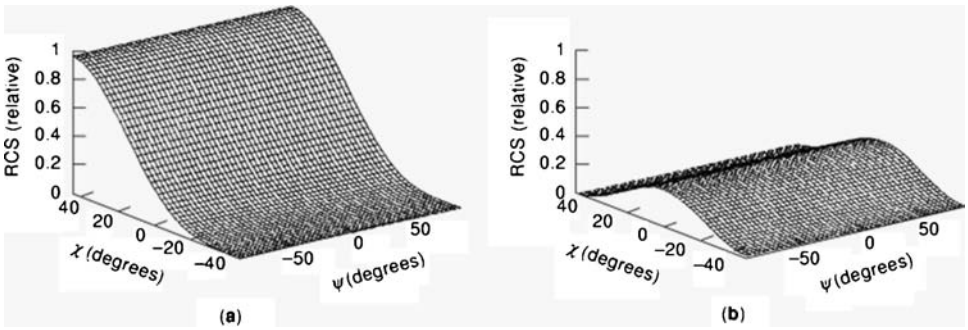

Figure 6. (a) Copolarized signature for a left-handed helix. The copolarized RCS is maximized by left-handed circular polarization and vanishes for right-handed circular polarization. (b) Cross-polarized signature of a left-handed helix. The cross-polarized response is maximized with linear polarizations, but the peak response is weaker than the maximum exhibited in the copolarized case.

distinctive and can be used to broadly classify targets. Two types of signatures are used: the co-polarized signature, in which the incident and scattered polarization states are assumed to be identical; and the cross-polarized signature, in which the incident and scattered states are assumed to be orthogonal. The signatures of some common targets are shown in Figs. 4–6.

Example 4. (Sphere) The co- and cross-polarized signatures of a sphere are shown in Figs. 4a and 4b, respectively. The signature consists of a plot of the target RCS versus the ellipticity and orientation angles χ and ψ of the incident and scattered radiation. Linearly polarized states lie along the $\chi = 0^\circ$ line, with vertical located at ($\chi = 0^\circ$, $\psi = \pm 90^\circ$) and horizontal located at ($\chi = 0^\circ$, $\psi = 0^\circ$). Left- and

right-handed circular polarizations are located along the $\chi = \pm 45^\circ$ lines. The ridge in the copolarized surface along the $\chi = 0^\circ$ line indicates that the copolarized RCS of the sphere is maximized when the polarization is linear. The response vanishes when circular polarization is used. (For this reason, some operational radar systems use circular polarization when monitoring targets through rain. This choice of polarization reduces the clutter signal produced by raindrops, which are roughly spherical in shape.) In contrast, the cross-polarized response is minimized by linear polarization and maximized when circular polarization is used. The surfaces in Fig. 4 are also the polarization signatures of a trihedral corner reflector and a flat plate at normal incidence, since these targets have the same normalized scattering matrices as the sphere [Eq. (20)].

Example 5. (Dihedral Corner Reflector) Figures 5a and 5b show the co- and cross-polarized responses, respectively, of a dihedral corner reflector with its seam oriented parallel to the horizontal plane. The copolarized RCS is maximum for vertical, horizontal, and circular polarizations, but vanishes for linear polarized radiation with an orientation angle $\psi = \pm 45^\circ$. Examination of the dihedral scattering matrix [Eq. (21)], shows that when the incident polarization state is linear with $\psi = \pm 45^\circ$, the scattered and incident polarization states are orthogonal. The copolarized response consequently vanishes, while the cross-polarized response (Fig. 5b), exhibits maxima at these points.

Example 6. (Helix) The co- and cross-polarized signatures of a left-handed helix are shown in Figs. 6a and 6b, respectively. The co-polarized RCS is maximized when left-hand circular polarization is used and vanishes for right-hand circular polarization. Unlike for the sphere or the dihedral corner reflector, the cross-polarized response of the helix never achieves a value of 1.

POLARIMETRIC RADAR DESIGN

A polarimetric radar, or polarimeter, measures the scattering matrix of a target by sequentially transmitting a pair of orthogonally polarized pulses toward the target and simultaneously measuring the co- and cross-polarized components of the scattered wave. The need to transmit and receive multiple polarizations makes the design of a polarimetric radar more complicated than the design of a conventional, single polarization, radar system. A basic polarimeter is composed of a transmitter that generates microwave pulses at a specified carrier frequency, an antenna capable of transmitting and receiving two orthogonally polarized wave components and focusing these waves into a narrow angular beamwidth in space, switching circuitry that alternately routes the transmitted pulses between the two orthogonal ports of the antenna feed, a pair of receivers for detecting the signals received from the antenna, and a multichannel data acquisition system for recording the signals backscattered from the target.

As in conventional radar design, the most important design equation for radar polarimetry is the radar range equation

$$\text{SNR} = \frac{P_t G_t \sigma A}{(4\pi)^2 R^4 k T B F_n} \tag{35}$$

which gives the receiver signal-to-noise ratio (SNR) in terms of the peak transmitted power level P_t; the antenna gain, $G_t = 4\pi/\theta^2$, where θ is the antenna's focusing beamwidth (assumed here to be equal in azimuth and elevation planes, as is the case for a pencil-beam antenna); the antenna's collecting area A, which typically ranges between 60% and 95% of its physical area, depending on the aperture illumination efficiency; the polarization-dependent radar cross section of the target σ; the range between the radar antenna and the target R; the bandwidth B and noise figure F_n of the receiver; Boltzmann's constant, $k = 1.38 \times 10^{-23}$ J/K; and the physical temperature of the receiver T, usually taken to be 290 K. Whereas reliable radar target detection can often be accomplished with a receiver SNR of 15 dB using a conventional radar (7), measuring the polarimetric response of a target typically requires SNR levels of 20 dB or higher (8). A large part of polarimeter system design involves trading off the various parameters of Eq. (35) to achieve a specified level of SNR performance. Reference 2 describes some of the tradeoffs involved in the design of a spaceborne imaging radar polarimeter having transmitted power level $P_t = 5$ kW, antenna gain $G_t = 10{,}000$ (40 dB), and surface area $A = 32$ m^2 (15 dB) that achieves an SNR level of 24 dB when viewing Earth's surface at 400 km range. Another example of a spaceborne imaging polarimeter is given in Ref. 9.

The operating wavelength of a polarimetric radar system is chosen as the result of a tradeoff among considerations such as the physical size of the antenna, peak transmitted power level, availability of components, cost, and for most remote sensing applications, the sensitivity of the surface backscatter coefficient [or normalized radar cross section (NRCS)] to environmental parameters. In general, radar systems operating at higher microwave frequencies have smaller antennas and larger peak transmitted power levels than do radars operating at lower microwave frequencies. The focusing gain and physical size of an antenna are related by the equation $A = \lambda^2 G_t/4\pi$ (assuming 100% aperture efficiency), where wavelength λ is inversely related to the operating frequency f by the equation $\lambda = c/f$, where c is the speed of light. These equations reveal that larger antenna gains can be obtained for a given antenna size at higher frequencies than at lower frequencies. Conversely, a specified amount of focusing gain can be achieved with a smaller physical antenna size at a higher frequency than at a lower frequency. However, receiver SNR is proportional to the product of the focusing gain and the physical collecting area of the antenna. Therefore, increasing the operating frequency to reduce the physical size of an antenna while achieving a specified level of antenna gain results in reduced receiver SNR. This loss must be compensated by increasing the peak transmitted power level of the radar system. This tradeoff is particularly important in airborne and spaceborne radar system deployments where it is desirable to utilize small antennas.

At millimeter-wave frequencies and higher microwave frequencies (typically above X band), atmospheric attenuation becomes an important consideration, and the SNR in Eq. (35) must be multiplied by the term $\exp(-2\alpha R)$, where α, having units of nepers (napiers) per meter (Np/m), is the

attenuation coefficient. Attenuation coefficients for propagation through the clear atmosphere and through rain are given in Ref. 10 for different frequencies. When scattering targets are small compared with the operating wavelength, such as raindrops observed with a millimeter-wave radar system, σ is a strong function of frequency and is given by the Rayleigh expression $\sigma = a/\lambda^4$, where the constant a depends on the shape of the target. The SNR in this case is given by the equation

$$\text{SNR} = \frac{P_t G_t^2 \alpha \exp(-2\alpha R)}{(4\pi)^3 R^4 k T B F_n \lambda^2} \qquad (36)$$

which reveals that increases in the operating frequency (decreases in wavelength) result in higher SNR levels relative to operating at a lower operating frequency. Reference 11 describes a dual-frequency polarimetric radar system developed for cloud profiling studies. The radar contains transmitters operating at 33 and 95 GHz that share a common 1-m-diameter dielectric lens antenna. Because of the strong wavelength dependence in the backscatter coefficient from the raindrops, the 33-GHz channel of this radar requires 120 kW peak power level, whereas the 95-GHz channel requires only 1.5 kW peak power level to achieve the same SNR.

Transmitter Design Considerations

Polarimetric processing of radar data involves the coherent combination of scattered wave measurements corresponding to a pair of consecutive transmitted pulses. Phase-coherent transmitters are therefore used in most polarimetric radar designs. (A technique for measuring the time-averaged Mueller matrix directly that does not require a coherent transmitter is described in Ref. 5.) The master oscillator power amplifier (MOPA) transmitter configuration is commonly used in coherent transmitter design. In this configuration, a low-power (typically in the tens of milliwatts) microwave signal, derived from a microwave oscillator that is phase-locked to a stable crystal oscillator, is pulse-modulated using a pin diode switch and then amplified to achieve the required peak power level using a power amplifier. Solid-state field-effect transistor (FET) amplifiers are often used in lower frequency (X-band and below) microwave systems having power levels of several watts. Microwave power tube amplifiers [TWTs (traveling-wave tubes) and klystrons] are often used in higher-power and microwave frequency radar transmitters. Examples of polarimeter systems utilizing klystron amplifiers with peak power levels of 200 kW at S band and 1.5 kW at 95 GHz are described in Refs. 11 and 12, respectively. MOPA transmitters tend to be expensive, typically costing several tens to hundreds of thousands of dollars. These systems provide for highly flexible transmitted waveforms, however, and a variety of waveforms (pulsed, chirped, phase-coded) can be generated using a MOPA design.

Self-excited power oscillator tubes, such as the magnetron oscillator and the extended interaction oscillator (EIO), are also used in polarimeter transmitter designs. These devices often cost considerably less than MOPA transmitters, but they are typically limited to pulsed applications. These incoherent power oscillators typically exhibit frequency drift and pulse-to-pulse phase modulations, and frequency stabilization and coherent-on-receive circuits are required when these devices are used in polarimetric radar designs. Reference 11 gives an example of a high-power magnetron transmitter for a millimeter-wave polarimeter system.

Polarimeter Antennas

Polarimetric radar antennas must be capable of transmitting and receiving two orthogonally polarized waves. Any pair of orthogonal polarizations can be used, but vertical/horizontal linear and right/left circular are the most common. As in a conventional radar, the physical size of the antenna must be large enough to achieve the focusing beamwidth and directive gain specified by the system design and SNR budget, and the antenna sidelobes must be below some specified value. The antenna designs used in radar polarimeters must also achieve high polarization purity. A typical specification requires the cross-polarized radiation, integrated across the antenna pattern, to be 30 dB below the copolarized signal level (8).

Many of the antennas used for conventional radar design can be used in polarimeter systems by adapting them for dual-polarization operation. A corrugated horn antenna equipped with an orthomode transducer (OMT) can be used for dual-linear polarization operation in applications requiring modest directive gain (up to 20 dB). Higher levels of directive gain can be achieved by using the corrugated horn to illuminate a parabolic reflector in either a prime-focus or Cassegrain configuration (13, 14). References 11 and 15 describe millimeter-wave polarimeter systems that use dielectric lens antennas. The antenna for the polarimetric radar flown on the space shuttle, the *Spaceborne Imaging Radar*—C (SIR-C), is a microstrip patch array with transmit/receive (T/R) modules distributed across the array surface (9). The system operates simultaneously at L and C bands.

Polarization Switches

Single-pole double-throw (SPDT) switches are needed in the transmitter of a polarimetric radar to alternately route the transmitted signal between the two ports of the antenna. The switching is performed on a pulse-to-pulse basis, so the switches must be capable of toggling the high-power microwave-transmitted pulse between the two antenna ports at switching speeds of 0.1–1 ms or faster. For low-power (less than 10 W), short-range polarimeter designs, pin diode switches are often used. Higher-power applications (up to tens or hundreds of watts of peak transmitted power level) typically use ferrite switching circulators. Three circulators are typically used in the design, as described in Ref. 14. Off-the-shelf ferrite switching circulators capable of handling several tens of kilowatts are commonly available at L- through Ku-band microwave frequencies at a cost of several thousand dollars per circulator.

Many polarimeter designs require peak transmitter power levels that are too high for off-the-shelf ferrite switches. Reference 14 describes a high-power, 1-MW S-band polarimeter design that uses a ferrite switching circulator custom-made at a cost of $75,000. Reference 11 de-

scribes a 33-GHz, 125-kW polarimeter that uses two separate transmitters to feed the antenna ports, rather than a single transmitter with a polarization switch.

Receiver and Data Acquisition

Two superheterodyne receiving channels are used in a polarimeter to detect the co- and cross-polarized components of the scattered wave. Current designs achieve dynamic ranges of up to 100 dB by using low-noise front-end amplifiers, matched filters, and wide-dynamic-range coherent detectors. Standard in-phase/quadrature demodulator circuits operate over a limited dynamic range, typically on the order of 30 dB. The wide-dynamic-range circuits used in many polarimeter receivers use logarithmic detectors for measuring signal amplitude and constant-phase limiters followed by in-phase/quadrature demodulators for measuring signal phase. Examples of these detector circuits are given in Refs. 11 and 14. Data acquisition systems with six channels are required in polarimeters that utilize these wide-dynamic-range detectors.

Polarimeter Calibration

Calibration is an important aspect of polarimetric radar design that has received considerable attention in recent years. In order to determine the scattering or Mueller matrix of a target, accurate measurements of the relative magnitudes and phases of the EM fields constituting the target echo are needed. However, the estimates of these quantities that the radar system produces are inevitably contaminated by the system itself, due to component mismatch and/or a lack of polarization isolation. Without a proper calibration, the fixed biases (errors) in the measured magnitudes and phases introduced by the system cannot be differentiated from the true radar response of target. The objective of calibration is thus to determine the gain (magnitude and phase) of the four different measurement paths (vertical transmitter–vertical receiver; vertical transmitter–horizontal receiver; horizontal transmitter–horizontal receiver; and horizontal transmitter–vertical receiver) followed by the radar pulse during measurement of a target's scattering matrix, as well as to estimate the degree of cross-polarization distortion caused by the transmitting and receiving antennas. Once these calibration measurements are made, the contribution of the system to any target measurement can be determined and removed. One technique that is commonly used is to measure the polarimetric scattering behavior of three reference targets having known scattering matrices. The measurements so obtained provide enough information to uniquely determine the set of seven complex unknowns in the polarimeter distortion matrices required for polarimetrically calibrating the radar system (16). Other calibration techniques have been developed that invoke assumptions about the observed targets, such as reciprocity and uncorrelated co- and cross-polarized scattering, to estimate the system distortion matrices directly, without relying on reference scattering targets (17). A procedure for field calibration of bistatic polarimeter systems without using reference scattering targets has also been developed (18). For a summary of polarimetric calibration procedures, see Ref. 19.

CURRENT RESEARCH

Radar Scattering Studies

Polarimetric radar measurements can often be used to determine the physical scattering mechanisms responsible for a radar echo. As discussed in a previous section, a sphere and a trihedral corner reflector are examples of "odd-bounce scatterers" that exhibit scattering matrices having elements S_{vv} and S_{hh} in phase with each other. A dihedral corner reflector, in contrast, is an example of an "even-bounce scatterer", in which the S_{vv} and S_{hh} elements exhibit a 180° phase difference. In the case of the Mueller matrix, the elements L_{33} and L_{44} convey similar information. A complex radar target dominated by a single-bounce scattering mechanism exhibits large positive values for elements L_{33} and L_{44}, whereas these elements are negative when the target is dominated by a double-bounce scattering mechanism. In contrast, the Mueller matrix of a target composed of a combination of even- and odd-bounce scatterers exhibits near-zero values for L_{33} and L_{44} (20).

The mechanisms responsible for radar backscatter from the sea surface are a topic of current investigations. McLaughlin et al. (13) describe measurements of ocean waves in the Chesapeake Bay performed at a 3° grazing angle using a high-range-resolution (1.5-m) X-band polarimetric radar. These measurements were conducted to determine the physical scattering mechanisms responsible for *sea spikes*, which are strong radar echoes with anomalous polarization characteristics that occur in low-grazing-angle radar backscatter from the ocean surface. Figure 7 shows a typical copolarization signature of the ocean surface echo in the absence of a sea spike. The plot exhibits maximum RCS at VV polarization, minimum RCS at HH polarization, and intermediate cross sections of approximately 0.25, corresponding to a level 6 dB below the VV peak, at right-hand and left-hand circular polarizations. The *coefficient of variation*, a measure of the polarization sensitivity of a scatterer, is defined as the ratio of minimum to maximum RCS in a polarization signature plot (6). The coefficient of variation of this plot is 0.01 (−20 dB), indicating that the radar echo is highly polarized. The Mueller matrix (not shown) exhibited large values for L_{33} and L_{44}, meaning that a single-scattering mechanism, such as distributed *Bragg scattering*, dominates the radar echo from the ocean surface. Figure 8 shows a copolarization signature for a sea spike radar echo that occurred during the passage of a long ocean wave crest through the radar resolution cell. The sea spike echo exhibits polarimetric scattering characteristics that are substantially different from the ocean surface echo in the absence of sea spikes. Figure 8 exhibits RCS maxima at VV and HH polarizations as well as a large "pedestal" corresponding to relatively high cross-section values at other copolarization states. The coefficient of variation for this plot is 0.3 (−5.2 dB), a relatively large value, meaning that the echo is weakly polarization-sensitive. The L_{33} and L_{44} Mueller matrix elements for this echo had small values indicating that no single scattering mechanism dominates the backscatter signal. One possi-

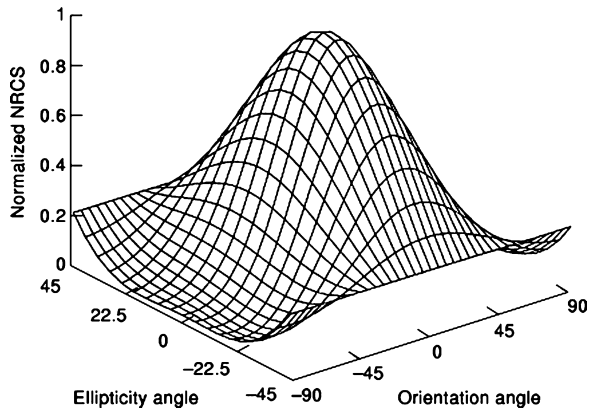

Figure 7. Copolarized signature of the sea surface in the absence of sea spikes. The high RCS at vertical polarization, the minimum at horizontal polarization, and the high degree of polarization (low pedestal) indicate a single, Bragg-like scattering mechanism.

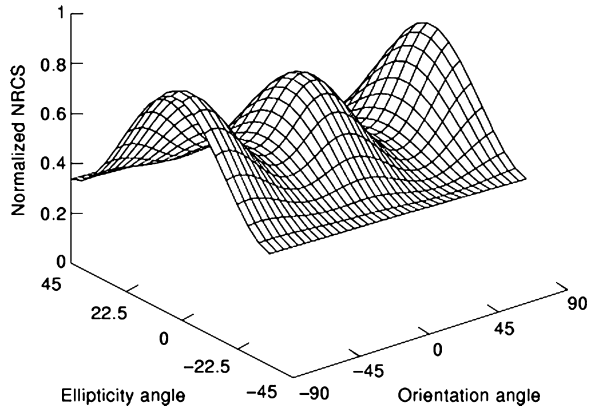

Figure 8. Copolarized signature of the sea surface in the presence of a sea spike. Peaks in the response at both vertical and horizontal polarizations and the low degree of polarization (high pedestal) indicate a mixture of scattering mechanisms.

ble explanation for this observation is that a combination of Bragg resonant waves and non-Bragg scatterers, such as plumes generated at breaking wavecrests, combine to form the sea spike echo from the ocean surface.

Sletten et al. (21) have also utilized a polarimetric radar to investigate sea spikes. In their experiments, an *ultrawideband*, polarimetric radar system was used to investigate the backscatter from breaking water waves generated in a laboratory wavetank. (The term *ultrawideband* refers to the ability of a radar to measure the backscatter from a target over a wide band of radar frequencies simultaneously.) Observed differences in the VV and HH responses as a function of radar frequency indicate that the strongest echoes (sea spikes) produced by the breakers are the result of a double-bounce scattering mechanism, arising from multiple scatter between the front face of the wave and a plume near its crest. In particular, the VV and HH frequency responses were found to be roughly complementary (i.e., HH high when VV is low, and vice versa), a result related to the 180° phase shift observed between S_{hh} and S_{vv} for double-bounce scatterers.

Image Classification

Another active area of research is image classification. In remote sensing, the objective of this research is to automatically separate different regions of an image into different classes, dependent on the type of terrain or land usage. For instance, classification schemes are under development to separate forested, urban, agricultural, and water-covered regions in remotely sensed imagery. In an ideal classification scheme, the signal characteristics that define each class can be uniquely associated with physical attributes of the scatterers in that class. Polarimetric images are the best candidates for this type of processing, given the amount of information they provide on the scatterers in the scene. Signal polarization constitutes another dimension in which distinctions can be drawn between regions in an image. The same principle can be applied to the problem of detecting and classifying targets (as opposed to regions within an image) with a nonimaging radar. This is the situation encountered in some military applications.

Polarimetric target decomposition is one approach to classification. In this approach, the scattering, Mueller, or coherency matrix is considered to be a linear combination of several basis matrices, each of which represents a canonical target or a departure of the original matrix from the canonical target. In any radar image of a real surface, the signal for a given pixel is produced by several (perhaps many) scattering centers or objects within the illuminated scene. The total signal is a mixture of the echoes produced by each scattering center, and thus the polarimetric properties of that pixel are a mixture as well. In addition, motion of the scatterers (due to surface winds, e.g.) may cause variation in their scattering properties, resulting in partial polarization. Target decomposition techniques attempt to break the measured matrices down into their fundamental constituents or to extract the characteristics of the primary scattering centers from the background.

The application of polarimetric decomposition theories to radar problems began with the pioneering work of Huynen (22). Huynen decomposed the coherency matrix into two components: a pure (i.e., completely polarized) target, and a mixed (partially polarized) state that was invariant to rotations of the radar system about the line of sight. The pure target is intended to represent the average, or dominant, target, and the mixed state is the residue or remainder. Enforcing rotational invariance on the residue ensures, at least to some degree, that the mixed state has no preferred axis of symmetry and is thus produced by the unpolarized noise in the measurement. Holm and Barnes (23) later determined that there are actually two other Huynen-like decompositions of the coherency matrix, which makes interpretation of the results somewhat ambiguous. Holm and Barnes also developed another decomposition method, referred to as the "natural" or "characteristic" decomposition, which breaks the coherency matrix into three components: a matrix representing a pure state that provides a measure of the average target; a mixed-state matrix, which indicates the variance of the target about its average; and an unpolarized component. This decomposition is based on an eigenvalue analysis of the coherency matrix and can thus be expected to produce statistically independent

components. In a simulation, this method was successfully used to extract a rotating dihedral corner reflector embedded in polarization noise. Krogager and Czyz (24) have taken a different approach to the decomposition problem, concentrating instead on decomposition of the scattering matrix. In this technique, the scattering matrix is decomposed into three coherent (nonaveraged) components that can be physically interpreted as representing a sphere, a rotated dihedral corner reflector, and a helix. While these three matrices are not orthogonal (the dihedral component can also be attributed to a pair of helices), the technique has physical appeal and may be a natural scheme for some applications. Freeman and Durden (25) have developed a three-component model comprising three mechanisms: volume scatter from a cloud of dipoles with random orientations, double-bounce scatter from two orthogonal surfaces with different dielectric constants, and a moderately rough surface modeled by Bragg scatter. A fit of this three-component model to imagery containing backscatter from a variety of vegetation and open water indicates that the model describes the actual scattering mechanisms well. Cloude and Pottier have summarized these and other decomposition techniques (26) and have introduced their own classification scheme based on an eigenvector decomposition of the coherency matrix (27). The technique classifies pixels within an image through two parameters: the polarimetric entropy H, which is derived from the eigenvalues of the coherency matrix and that indicates the degree of polarization; and an angle α, which indicates the dominant scattering mechanism. α ranges from 0° to 90°, with low values indicating geometric optics and higher values indicating Bragg scattering and double-bounce mechanisms. The authors divide the H–α plane into different zones, each of which indicates a different class of scattering behavior. The scheme is unsupervised (i.e., does not require training data), and the results of its application to imagery containing a mixture of vegetation, urban buildings, and open water are promising.

Other approaches to polarimetric image classification exist as well. For instance, Lee et al. (28) have applied a Bayes maximum-likelihood classifier to the problem, including the effects of multiple-look averaging, while Yueh (30) conducted a similar investigation assuming single-look statistics. Lee et al. (29) have also combined the unsupervised decomposition scheme of Cloude and Pottier with a maximum-likelihood classifier based on the complex Wishart distribution for the polarimetric covariance matrix. Ferrazzoli et al. (31) have used a simplified scheme that considers the normalized RCS values for five polarization combinations (HH, VV, HV, circular copolarized, and circular cross-polarized) and three radar frequency bands (P, L, and C) to distinguish between forest, urban areas, and agricultural areas and to classify several types of crops. Fully polarimetric synthetic aperture radar (SAR) imagery has also been classified using algorithms based on neural nets (see, for instance, Ref. 32).

Contrast Enhancement

The scattering environment observed by a radar system is composed of many different targets that scatter incident electromagnetic energy. To the extent that the different scatterers or classes of scatterers have different polarization signatures, the echoes from one type of scatterer may be enhanced relative to the echoes from other scatterers by using a polarimetric radar. As discussed earlier in this article, knowledge of the polarization scattering matrix or Mueller matrix of a target allows one to calculate the transmitting and receiving polarizations that would result in maximum or minimum radar cross-section level (33). It is also possible to simulate (synthesize) any desired receive polarization in the signal processor of a polarimetric radar by forming a weighted linear combination of the signals received by the two receiving channels (34). Similarly, it is possible to synthesize any arbitrary transmitting antenna polarization by forming a weighted linear combination of the received signals corresponding to two consecutive transmitted pulses. Therefore, the processor can synthesize the appropriate combination of transmitting and receiving antenna polarization states that maximize (or minimize) the echo from a given scatterer having a known polarization scattering matrix or Mueller matrix.

Figure 9 illustrates the concept of image contrast enhancement. Figures 9a, 9b, and 9c show SAR images of San Francisco, California processed using HH, VV, and VH=HV polarizations, respectively. The Golden Gate Bridge appears as a bright, vertical line in the middle third of the images, and Golden Gate Park is the wide, horizontal band that appears in the lower quadrant. A comparison of the three images shows that HH polarization maximizes the contrast between the developed, urban areas (recognized by a grid pattern formed by perpendicular streets) and Golden Gate Park, which contains mixed vegetation. VV polarization increases the relative RCS of the waves present on the surface of the Pacific Ocean, as seen by a comparison of Figs. 9a and 9b, while the image in Fig. 9c shows that maximum contrast between the land and water occurs for the HV(=VH) polarization combination. [The imaging polarimeter used to collect the data presented in Fig. 9, the NASA/JPL AIRSAR, was developed by the Jet Propulsion Laboratory (JPL). For more information on the system and its successors, see Refs. 2, 6, and 35].

For target detecting radars, it is desirable to enhance the radar echo from wanted targets, such as aircraft, while suppressing the echo from unwanted targets, such as terrain clutter. In certain imaging radar applications, it is desirable to enhance the echo from one type of terrain while suppressing the echo from other types of terrain. The limitations to contrast enhancement are (1) lack of a priori knowledge of the scattering matrix of the desired target and (2) similarity of polarimetric responses of the desired and undesired scattering targets. Research performed on the target detection problem, including techniques to adaptively estimate the scattering matrices of targets and clutter, is described in Refs. 36–38. Work in polarization-based suppression of bistatic clutter is described in Ref. 39. Several papers dealing with polarimetric contrast enhancement in imaging radars for terrain mapping are summarized in Ref. 2.

Figure 9. Synthetic aperture radar image of San Francisco, near Golden Gate Park, processed with three different polarization combinations: (a) HH polarization, showing the strongest contrast between urban and mixed vegetation areas; (b) VV polarization, which exhibits stronger backscatter from the areas covered by open water; and (c) HV = VH polarization, which maximizes the contrast between open water and land.

Meteorology

While Doppler (coherent) radar has become an indispensable tool for meteorologists, the current fleet of operational weather radars utilize a single polarization. Research has shown, however, that polarization-diverse radars can provide weather forecasters with additional information. For example, polarimetric radar systems can discriminate ice particles from water droplets, and can detect hail. Radar echoes from precipitation are complex and depend on the shape, size distribution, water-phase state, and type of hydrometeor responsible for scattering the incident energy (40). Large raindrops assume a flat pancake shape as they achieve terminal falling velocity, and thus scatter horizontally polarized energy more effectively than vertically polarized energy. Hailstones, in contrast, have irregular shapes but tumble as they fall, and thus exhibit equal scattering cross sections at vertical and horizontal polarizations. Exploiting this observation, Aydin et al. (41) developed a technique for discriminating rain from hail echoes by computing the ratio of horizontal to vertical power levels received when a dual-polarization radar transmits pulses into storms. Accurate measurement of rainfall rate is another important and evolving issue in the meteorological community. The relationship between the radar reflectivity coefficient of rain and the rain rate is different for different types of rain. Seliga and Bringi (42) have shown that independent measurement of rain reflectivity at vertical and horizontal polarizations provides more accurate rainfall estimates than do single-polarization radar estimates. Polarization diverse radars can also provide information on clouds. Mead (5) has developed a lightweight 94-GHz radar for airborne cloud profiling studies, and has used this system to determine the height of the melting layer. The technique involves calculation of the ratio of cross-polarized to copolarized scattering when looking vertically into a layer of developing clouds.

Topographic Mapping

Schuler et al. (43, 44) have developed a technique to extract topographic information from fully polarimetric radar imagery. The method extracts the azimuthal slope of the imaged terrain by determining the shift that this slope induces in the polarimetric response. Integration of the inferred slopes across the image, in conjunction with suitable tie points (integration constants), then yields the elevation profile. To illustrate the basic principle behind the technique, assume that the scattering from the surface can be described by Bragg scatter, and thus has a scattering matrix (in the absence of any azimuthal tilts) of the form

$$\bar{S} = \begin{bmatrix} a & 0 \\ 0 & b \end{bmatrix} \tag{37}$$

where a and b are real and $b>a$. If the surface is tilted in the azimuthal plane by an angle δ, the scattering matrix becomes

$$\bar{S} = \begin{bmatrix} \cos\delta & -\sin\delta \\ \sin\delta & \cos\delta \end{bmatrix} \cdot \begin{bmatrix} a & 0 \\ 0 & b \end{bmatrix} \cdot \begin{bmatrix} \cos\delta & \sin\delta \\ -\sin\delta & \cos\delta \end{bmatrix} \tag{38}$$

which, after carrying out the matrix multiplication, can be expressed as

$$\bar{S} = \begin{bmatrix} a\cos^2\delta + b\sin^2\delta & (a-b)\cos\delta\sin\delta \\ (a-b)\cos\delta\sin\delta & a\sin^2\delta + b\cos^2\delta \end{bmatrix} = \begin{bmatrix} \bar{S}_{\delta hh} & \bar{S}_{\delta hv} \\ \bar{S}_{\delta vh} & \bar{S}_{\delta vv} \end{bmatrix} \tag{39}$$

Tilting the surface introduces the off-diagonal terms $\bar{S}_{\delta hv}$ and $\bar{S}_{\delta vh}$, with $\bar{S}_{\delta hv} = \bar{S}_{\delta vh}$ from reciprocity. Solving this system of equations for δ produces the following expression:

$$\delta = \frac{1}{2}\tan^{-1}\left(\frac{2\bar{S}_{\delta vh}}{\bar{S}_{\delta hh} - \bar{S}_{\delta vv}}\right) \tag{40}$$

Thus, the azimuthal slope of the surface can be derived from the elements of the measured scattering matrix. While Eq. (40) applies only to the case of Bragg scattering and cannot be applied in general, it illustrates the basic principle behind the method. A more general technique for determining the shift in the polarimetric response, and thus the azimuthal slope, is discussed in Ref. 43.

Figure 10a shows an elevation map of the terrain near Camp Roberts, CA, derived from JPL AIRSAR data using this method (44). For comparison, a digital elevation map (DEM) of the same area derived from data collected with the JPL TOPSAR system, an interferometric SAR designed to measure terrain topography, is displayed in Fig. 10b. The overall form of the two maps agrees very well, as do

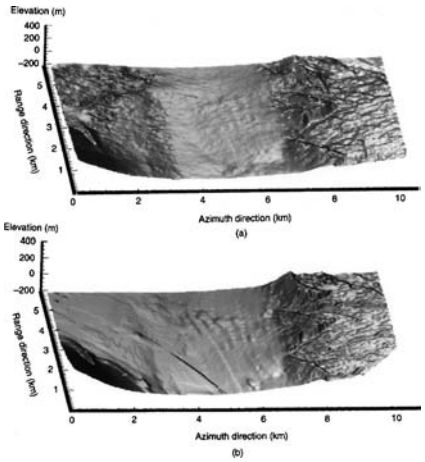

Figure 10. (a) Topographic map of Camp Roberts, CA produced from polarimetric SAR data collected by the JPL AIRSAR. The surface elevation is computed by integrating surface slopes derived from the polarimetric signature. Data from two orthogonal aircraft passes are used to reduce the number of required tie points to one. (b) Topographic map of the area in Fig. 10a produced using the JPL TOPSAR system. The RMS difference between the maps is 28 m.

many of the details. The RMS elevation difference between the maps over the entire region is 28 m, while the maximum and minimum elevations in the scene are 300 and 180 m, respectively. The errors in the polarimetrically derived map are greatest in the river valleys, where more complex, manmade structures are present. In order to reduce the required number of tie points to one, data from two orthogonal aircraft passes have been used. The final elevation map is obtained as an iterative solution to the Poisson equation using curvature data derived from the two passes as inputs (43).

BIBLIOGRAPHY

1. H. Mott, *Antennas for Radar and Communications—A Polarimetric Approach*, New York: Wiley, 1992. J. L. Eaves, and E. K. Reedy, eds., *Principles of Modern Radar*, Van Nostrand Reinhold, New York, 1987, Chapter 20.
2. F. T. Ulaby, and C. Elachi, eds., *Radar Polarimetry for Geoscience Applications*, Artech House, Boston, 1990.
3. J. R. Huynen, Measurement of the target scattering matrix, *Proc. IEEE* 936–946 (Aug. 1965) .
4. W. M. Boerner, H. Mott, E. Luneberg, C. Livingstone, B. Brisco, R. Brown, and J. S. Patterson, in:R. A. Reyerson, ed., *The Manual of Remote Sensing*, 3rd ed., ASPRS Publishing, Bethesda, MD, 1997, Chapter 5.
5. J. B. Mead and R. E. McIntosh, Millimeter wave radars for remotely sensing clouds and precipitation, *Proc. IEEE.* **82**(12): 1891–1906 (Dec. 1994) .
6. J. J. van Zyl, H. A. Zebker, and C. Elachi, Imaging radar polarization signatures: theory and observation, *Radio Sci.* **22**(4): 529–543(July– Aug 1987).
7. M. I. Skolnik, *Radar Handbook*, McGraw-Hill, New York, 1990.
8. P. C. Dubois, D. Evans, and J. van Zyl, Approach to derivation of SIR-C science requirements for calibration, *IEEE Trans Geosci. Remote Sens.* **30**(6): 1145–1149 (Nov. 1992) .
9. B. L. Huneycutt, Spaceborne imaging radar-C instrument, *IEEE Trans. Geosci. Remote Sens.* **27**(2): 164–169 (March 1989) .
10. F. T. Ulaby, R. K. Moore, and A. K. Fung, *Microwave Remote Sensing, Active and Passive*, Vol. 2, Artech House, Norwood, MA, 1986.
11. S. P. Lohmeier, S. M. Sekelsky, J. M. Firda, G. A. Sadowy, and R. E. McIntosh, Classification of particles in stratiform clouds using the 33 and 95 GHz polarimetric cloud profiling radar system (CPRS), *IEEE Trans. Geosci. Remote Sens.* **35**(2): 256–270 (March 1997) .
12. D. J. McLaughlin et al., Fully polarimetric bistatic radar scattering behavior of forested hills, *IEEE Trans. Anten. Propag.* **50**(2): 101–110 (Feb. 2002) .
13. D. J. McLaughlin, N. Allan, E. Twarog, and D. B. Trizna, High resolution polarimetric radar scattering measurements of log grazing angle sea clutter, *IEEE J. Ocean. Eng.* **20**(3): 166–178 (July 1995) .
14. J. Metcalf et al., *An 11-cm Full-Matrix Polarimetric Radar for Meteorological Research*,USAF Phillips Laboratory Geophysics Directorate, Environmental Research Paper PL-TR-91-2167, No. 1088, June 1991.
15. A. L. Pazmany, R. E. McIntosh, R. D. Kelly, and G. Vali, An airborne 95 GHz dual-polarized radar for cloud studies, *IEEE Trans. Geosci. Remote Sens.* **32**(4): 731–739 (July 1994) .
16. R. M. Barnes,*Polarimetric Calibration Using In-Scene Reflectors*,Report TT-65, MIT Lincoln Lab., Lexington, MA, 1986.
17. J. J. van Zyl, Calibration of polarimetric images using only image parameters and trihedral corner reflector responses, *IEEE Trans. Geosci. Remote Sens.* **28**: 337–348 (1990) .
18. D. J. McLaughlin, Z. Ren, and Y. Wu, A bistatic polarimeter calibration technique, *IEEE Trans. Geosci. Remote Sens.* **33**(3): 796–799 (May 1995) .
19. A. Freeman, SAR calibration: An overview, *IEEE Trans. Geosci. Remote Sens.* **30**: 1107–1121 (Nov. 1992) .
20. J. J. VanZyl, Unsupervised classification of scattering behavior using radar polarimetry data, *IEEE Trans. Geosci. Remote Sens.* **27**(1) (Jan. 1989) .
21. M. A. Sletten and D. B. Trizna, An ultrawideband, polarimetric radar for the study of sea scatter, *IEEE Trans. Anten. Propag.* **42**(11) (Nov. 1994) ; M. A. Sletten and J. Wu, Ultrawideband, polarimetric radar studies of breaking waves at low grazing angles, *Radio Sci.* **31**(1) (Jan.–Feb. 1996).
22. J. R. Huynen," Phenomenological theory of radar targets", inP. L. E. Uslenghi, ed., *Electromagnetic Scattering*, Academic Press, New York, 1978.
23. W. A. Holm and R. M. Barnes, On radar polarization mixed target state decomposition techniques, *Proc. 1988 IEEE Natl. Radar Conf.* 249–254.
24. E. Krogager and Z. H. Czyz, Properties of the sphere, diplane, helix decomposition, *Proc. 3rd Int. Workshop on Radar Polarimetry*, Nantes, France, March 21–23, 1995.
25. A. Freeman and S. Durden, A three component scattering model to describe polarimetric SAR data, *Radar Polarim. SPIE.* **1748**: 213–224 (1992) .
26. S. R. Cloude and E. Pottier, A review of target decomposition theorems in radar polarimetry, *IEEE Trans. Geosci. Remote Sens.* **34**(2): 498–518 (March 1996) .

27. S. R. Cloude and E. Pottier, An entropy based classification scheme for land applications of polarimetric SAR, *IEEE Trans. Geosci. Remote Sens.* **35**(1): 68–78 (Jan. 1997) .
28. J. S. Lee, M. R. Grunes, and R. Kwok, Classification of multilook polarimetric SAR imagery based on complex Wishart distribution, *Int. J. Remote Sens.* **15**(11): 2299–2311(July 20, 1994).
29. J. S. Lee, M. R. Grunes, T. L. Ainsworth, L. Du, D. L. Schuler, and S. R. Cloude, Unsupervised classification using polarimetric decomposition and the complex Wishart classifier, *IEEE Trans. Geosci. Remote Sens.* **37**(5): 2249–2258 (Sept. 1999) .
30. H. A. Yueh, A. A. Swartz, J. A. Kong, R. T. Shin, and L. M. Novak, Bayes classification of terrain cover using normalized polarimetric data, *J. Geophys. Res.* **93**(B12): 15261–15267(Dec. 10, 1988).
31. P. Ferrazzoli, S. Paloscia, P. Pampaloni, G. Schiavon, S. Sigismondi, and D. Solimimi, The potential of multifrequency polarimetric SAR in assessing agricultural and aboreous biomass, *IEEE Trans. Geosci. Remote Sens.* **35**(1): 5–17 (Jan. 1997) .
32. C.-T. Chen, K.-S. Chen, and J.-S. Lee, The use of fully polarimetric information for the fuzzy neural classification of SAR images, *IEEE Trans. Geosci. Remote Sens.* **41**(9): 2089–2100 (Sept. 2003) .
33. J. J. van Zyl, C. H. Papas, and C. Elachi, On the optimum polarizations of incoherently reflected waves, *IEEE Trans. Anten. Propag.* **AP-35**(7) (July 1987) .
34. D. Guili, Polarization diversity in radars, *Proc. IEEE.* **74**(2): 245–286 (Feb. 1986) .
35. H. A. Zebker, J. J. Van Zyl, S. L. Durden, and L. Norikane, Calibrated imaging radar polarimetry: technique, examples, and applications, *IEEE Trans. Geosci. Remote Sens.* **29**(6) (Nov. 1991) .
36. V. C. Vannicula and S. Lis," Polarization vector signal processing for radar clutter suppression", inW. M. Boerner et al., eds., *Inverse Methods in Electromagnetic Imaging*, Reidel, Hingham, MA, 1985, Vol. 2,pp. 739–770.
37. G. A. Ioiannidis and D. E. Hammers, Optimum antenna polarizations for target discrimination in clutter, *IEEE Trans. Anten. Propag.* **AP-27**: 357–363 (May 1979) .
38. L. M. Novak, M. B. Sechtin, and M. J. Cardullo, Studies of target detection algorithms that use polarimetric radar data, *IEEE Trans. Aerospace Electron. Syst.* **25**(2) (1989) .
39. D. J. McLaughlin and R. S. Raghavan, *A Study of Polarimetric Strategies for Suppressing Bistatic Clutter with Applications to Radar Detection*,USAF Rome Laboratory Contract F19628-93-k-0005, final report, June 1997.
40. M. Hall, ed., Special papers: Multiple parameter radar measurements of precipitation, *Radio Sci.***19** (1984) .
41. K. Aydin, T. Seliga, and V. Balaji, Remote sensing of hail with a dual linear polarization radar, *J. Clim. Appl. Meteorol.* **25**: 1475–1484 (1986) .
42. T. A. Seliga and V. N. Bringi, Potential use of radar differential reflectivity measurements at orthogonal polarizations for measuring precipitation, *J. Appl. Meteorol.* **15**: 69–76 (1976) .
43. D. L. Schuler et al., Topographic mapping using polarimetric SAR data, *Int. J. Remote Sens.* **19**(1): 141–160 (1998) .
44. D. L. Schuler et al., Terrain topography measurement using multipass polarimetric synthetic aperture radar data, *Radio Sci.* **35**(3): 813–832 (2000) .

MARK A. SLETTEN
DAVID J. MC LAUGHLIN

Naval Research Laboratory,
Washington, DC
University of Massachusetts,
Amherst, Massachusetts